# Soft Matter

Accepted Manuscript






ROYAL SOCIETY OF CHEMISTRY

www.rsc.org/softmatter

ARTICLE TYPE www. rsc.org/xxxxxx | XXXXXXXX

# Self-assembly of kagome lattices, entangled webs and linear fibers with vibrating patchy particles in two dimensions

**Gustavo A. Chapela,*[a] Orlando Guzmán,[a] José Adrián Martínez-González,[a,b] Pedro Díaz-Leyva,[a] and Jacqueline Quintana-H[c]**

***Received Xth XXXXXXXXXX 20XX, Accepted Xth XXXXXXXXX 20XX***
***First published on the web Xth XXXXXXXXXX 200X***
**DOI: 10.1039/b000000x**

A vibrating version of patchy particles in two dimensions is introduced to study self-assembly of kagome lattices, disordered networks of looping structures, and linear arrays. Discontinuous Molecular Dynamics simulations in the canonical ensemble are used to characterize the molecular architectures and thermodynamic conditions that result in each of those morphologies, as well as the time evolution of lattice formation. Several versions of the new model are tested and analysed in terms of their ability to produce kagome lattices. Due to molecular flexibility, particles with just attractive sites adopt a polarized-like configuration and assemble into linear arrays. Particles with additional repulsive sites are able to form kagome lattices, but at low temperature connect as entangled webs. Abundance of hexagonal motifs, required for the kagome lattice, is promoted even for very small repulsive sites but hindered when the attractive range is large. Differences in behavior between the new flexible model and previous ones based on rigid bodies offer opportunities to test and develop theories about the relative stability, kinetics of formation and mechanical response of the observed morphologies.

## 1 Introduction

Self-assembly is a reversible process that can be controlled by proper design of pre-existing components.[1] Self-assembly of colloidal particles is the spontaneous formation of meso and macroscopic structures starting from individual building blocks designed for that purpose. Being able to predict what building block will create a designed structure is an important premise for the development of new materials. Colloidal materials are an important part of this endeavour, with useful applications as catalytic supports, biomaterials, photonics and lightweight structural components.

A kagome lattice, named by I. Syosi after a Japanese woven bamboo-basket pattern,[2] is characterized by interlaced triangular and hexagonal shapes. The experimental formation of kagome lattices from simple colloidal triblock Janus particles, as reported by Chen *et al.*,[3] is an important achievement. In the laboratory, triblock colloids are built with two hydrophobic poles and a central hydrophilic tropical portion; the hydrophobic effect of the poles gives rise to an attractive interaction between them. The tropical hydrophilic region is charged, but adding salt screens electrostatic repulsions and allows the hydrophobic attraction to come into play. The two hydrophobic poles are designed to allow only two nearest neighbors by pole; this is accomplished by poles subtending an angle of 65 degrees. The triblock colloids produce a stack of highly porous, two dimensional kagome lattices against the bottom of the experimental container. Obtaining such open lattices directly from self-assembly avoids the template-assisted procedure used by Xia *et al.*[4]

Since the seminal work by Chen *et al.*[3] a large body of experimental,[5–22], theoretical[23–26] and computational simulation[27–36] work has been developed and reviewed.[37–40] Granick's group has made further experimental contributions to the field,[5–7] introducing new fabrication methods that control patch size and position,[5] as well as the number of patches and particle elongation,[6,10] aimed to obtain new classes of open lattices and clusters. They attained a variety of three-dimensional structures in a staged manner, out of tetrahedral clusters assembled from patchy particles.[7] In addition to other techniques for the fabrication of patchy particles,[11,12] the work by Sacanna *et al.*[15] about particles with magnetic patches should be highlighted because of the ability to change the assembled pattern upon application of an external magnetic field.

On the theoretical side, although Edlund *et al.*[41] have provided a method to design isotropic interactions in order to obtain a given lattice, it is important to address the anisotropic character of the interactions of patchy particles forming open lattices. A theoretical study of the kagome lattice formed by

[a] *Departamento de Física, Universidad Autónoma Metropolitana-Iztapalapa, Av. San Rafael Atlixco 186, Col. Vicentina, 09340 México D.F., México. gchapela@xanum.uam.mx*
[b] *(Present address) Institute for Molecular Engineering, The University of Chicago, Chicago, Illinois 60637, USA.*
[c] *Instituto de Química. Universidad Nacional Autónoma de México. Apdo. Postal 70213, 04510 Coyoacán, México, D.F., México.*

triblock Janus particles, presented by Mao *et al.*[23] and further developed by Mao,[24] found that entropic effects account for the mechanical and thermodynamical stability of these assemblies: rotational entropy explained the former, while reduction of the Helmholtz free energy due to entropy of vibrational modes of the lattice accounted for the latter.

These experiments and theoretical models consider patchy particles as essentially rigid bodies. Nanoscopic objects such as proteins and other biopolymers also have hydrophilic and hydrophobic regions and self-assemble readily, but they are flexible. It is important to investigate the effect of flexibility on the relative stability of different types of open lattices and fluid phases. As a first step in this direction, the following question may be asked: can a simple flexible model, such as a central hard core decorated with vibrating SW sites, form kagome lattices? To what extent is steric stabilization needed to prevent the formation of a closed-pack lattice instead?

This far, simulation searches for lattice-forming systems seem also dedicated exclusively to rigid particles. In 3D simulations no kagome network has been found yet, although diverse phases and morphologies have been reported: numerical simulations using two-patch particles are presented by Giacometti *et al.*;[42] they obtained a succession of closed-pack crystals, planes and chains by changing the size of the patches. Preisler *et al.* simulated one-patch Janus particles that form long and metastable tubular arrays in 3D.[32] The 3D simulation of a triblock model by Romano and Sciortino produced a crystal formed by stacks of planar rectangular lattices;[33] they also reported that a pure tetrastack lattice, with possible photonic properties, was spontaneously crystallized[34]. No kagome lattice is obtained in these 3D simulations. Their interpretation of this fact is that the presence of an external field is a necessary condition to form a 2D kagome crystal in a 3D simulation. It must be emphasized that in the actual 3D laboratory experiment several layers of a 2D kagome network are formed.

Still, there are simulations of several rigid-body models that form kagome lattices in systems with reduced dimensionality: isotropic particles confined to a plane[41], the surface of a sphere[36] or the first molecular layer next to a wall;[29] as well as triblock Janus particles in quasi 2D,[9,33] where the particles have their centers confined to a plane, but they are allowed to rotate three-dimensionally. Of these works, only the one by Romano *et al.*[33] gives a complete phase diagram for its models, consisting of two triblock patchy particles with an opening angle of 32.9 and 58.4 degrees.

In this work, discontinuous molecular dynamics simulations (DMD) in two dimensions are performed using a new type of model, with flexible particles that are able to self-assemble into kagome lattices (as well as other structures). The new models use multi-site particles formed by a central hard disk (HD) decorated with smaller, vibrating square well (SW) or HD sites. The latter sites imitate the hydrophobic and hydrophilic interactions in the experimental colloidal system. The new model is introduced in a detailed way below. The vibrating patches are similar to their rigid counterparts in the sense that, on average, they cover a similar attractive area (or volume, if simulated in three dimensions). The DMD simulations, with the new type of model, allow us to calculate the phase diagram, the structure of the different phases, as well as the kinetic process by which the kagome lattice is formed.

Several different models of vibrating patchy particles in 3D are tried in order to obtain a kagome lattice. More than 400 simulation runs are performed but none of them formed an open network. The results of these simulations are outside the scope of this work and will be communicated separately.

## 2 Interaction models

Two different models, based in the vibrating SW potential for molecules,[43,44] are used in this work, depicted in Fig. 1. They are formed by a central HD particle decorated by two or four smaller interaction sites.

The first model with two sites (M2) is shown in the left panel of Fig. 1. It is formed by a central HD of diameter $\sigma$, with two smaller SW disks located at a distance $L_{SW}$ from the center of the large disk. The SW potential has a depth $\varepsilon_{SW}$ and range $\lambda_{SW}$. In order to keep the geometry of the molecule constant the smaller sites are trapped in two infinite-depth potential wells that keep them vibrating at an average distance $L_{SW}$ from the large disk center (and a distance $2L_{SW}$ form each other). The maximum amplitude of the vibration is $L_{VW}$. The detailed definition of the trapping and interaction potentials is given in the Appendix.

For the values of the SW potentials used in this work, most of the attractive volume is buried inside the hard central particle, leaving only a small "patch" of angular size $\theta_{SW}$ available for assembly. This angle corresponds to an angle spanned by the intersection of the central HD with the SW attractive potential, as indicated in Fig. 1. The extreme of the attractive potential protrudes a distance $\delta_{SW}$ from the central HD. The values of $\delta_{SW}$ and $\theta_{SW}$ are fixed by the distance $L_{SW}$ and the sizes of the central HD and SW sites.

The second model (M4) (right panel Fig. 1) is the same as model M2 but with two HD sites with diameter $\sigma_{HD}$ added at a 90 degree angle from the first pair, constrained to an average distance $L_{HD}$ from the central HD and also constrained to an average distance $L_{SW-HD}$ from the two smaller SW disks (their maximum amplitude of vibration is also $L_{VW}$).

In the middle and lower parts of Fig. 1 a schematic plot of the intramolecular (middle) and intermolecular (bottom) potentials is given. The intramolecular potentials show the trapping potentials among the different components of each model and the intermolecular potentials include the SW and HD potentials. For model M2 the intramolecular trapping potentials

at $L_{SW}$ and at $2L_{SW}$ are shown and for model M4 the extra trapping well at $L_{SW-HD}$ is shown also. The intermolecular potentials for the Large HD and the smaller SW patchys for model M2 are show. In the case of model M4 the extra intermolecular potentials for the smaller HD patchys are also shown. Intramolecular and intermolecular potentials are treated separately in the simulation program to avoid overlaps.

Reduced units are defined with $\varepsilon_{SW}$ and $\sigma$ as the units of energy and distance, respectively. Reduced variables are denoted with a star. Hence, the reduced molecular number density $\rho^* = \rho\sigma^2$ where the molecular number density $\rho = N_m/A$ with $N_m$ the number of patchy molecules and $A$ the area of the simulation box. The reduced time is defined as $t^* = \sigma\sqrt{(m/\varepsilon_{SW})}$ with $m$ the mass of the patchy molecule.

Seven versions of the M2 model, given in Table 1, were extensively tested in this work for the formation of kagome structures. The first three versions (V1-V3) have a common value of the SW trapping distance $L^*_{SW}$ and increasing values of the range $\lambda^*_{SW}$. The remaining versions (V4-V7) have the same protruding distance $\delta^*_{SW} = 0.05$ and increasing range $\lambda^*_{SW}$. Thus, exploring the variation of $\lambda^*_{SW}$ keeping first $L^*_{SW}$ constant and then for constant $\delta^*_{SW}$ are the main aim of these series.

**Table 1** Reduced parameters for seven versions of the M2 model: SW range $\lambda^*_{SW}$, SW trapping distance $L^*_{SW}$, subtended angle $\theta_{SW}$ and protruding distance $\delta^*_{SW}$.

| *Ver* | $\lambda^*_{SW}$ | $L^*_{SW}$ | $\theta_{SW}$ | $\delta^*_{SW}$ |
|---|---|---|---|---|
| *V*1 | 0.3 | 0.45 | 34.3 | 0.1 |
| *V*2 | 0.4 | 0.45 | 47.1 | 0.15 |
| *V*3 | 0.5 | 0.45 | 59.9 | 0.2 |
| *V*4 | 0.4 | 0.35 | 36.4 | 0.05 |
| *V*5 | 0.6 | 0.25 | 54.3 | 0.05 |
| *V*6 | 0.7 | 0.20 | 66.2 | 0.05 |
| *V*7 | 0.8 | 0.15 | 82.8 | 0.05 |

The basic M4 model studied here (version V8) is similar to version V1 of the M2 model, with the additional parameters of HD-site diameter $\sigma^*_{HD} = 0.5$ and trapping distance $L^*_{HD} = 0.45$. Versions V9 to V14 have increasing values of the HD-site diameter, keeping other parameters as in V8. Finally, versions V15 and V16 differ by the value of the SW range but have the same protruding distance $\delta^*_{SW}$.

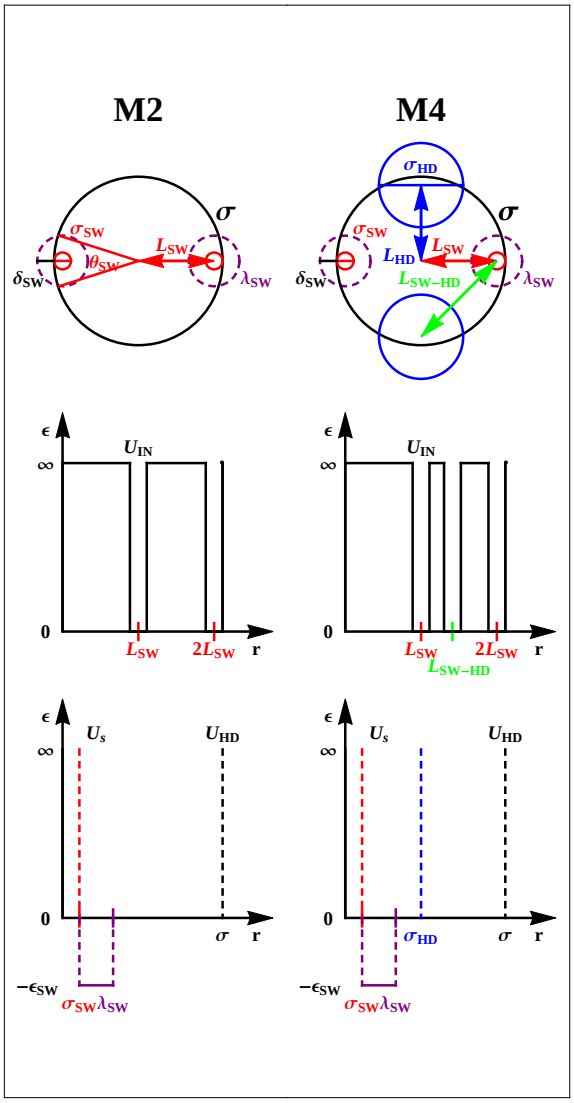


**Fig. 1** Vibrating patchy models with two (M2) and four sites (M4). On top, a graphic depiction of each model is given. The two bottom pictures represent the infinite SW potentials used to keep the molecular geometry, by trapping each site around its designated position. $U_{HD}$, $U_{IN}$ and $U_S$ are defined in the Appendix.

## 3 Discrete MD simulation details

Simulations are performed in the NVT ensemble, with 256 molecules. This corresponds to 768 particles (that is, the HD central particles and the vibrating sites) for model M2 and

**Table 2** Reduced parameters for ten versions of the M4 model: SW range $\lambda^*_{SW}$, SW trapping distance $L^*_{SW}$, subtended angle $\theta_{SW}$, protruding distance $\delta^*_{SW}$, HD-site diameter $\sigma^*_{HD}$, and HD-site trapping distance $L^*_{HD}$.

| *Ver* | $\lambda^*_{SW}$ | $L^*_{SW}$ | $\theta_{SW}$ | $\delta^*_{SW}$ | $\sigma^*_{HD}$ | $L^*_{HD}$ |
|---|---|---|---|---|---|---|
| *V*8 | 0.3 | 0.45 | 34.3 | 0.1 | 0.50 | 0.45 |
| *V*9 | 0.3 | 0.45 | 34.3 | 0.1 | 0.01 | 0.45 |
| *V*10 | 0.3 | 0.45 | 34.3 | 0.1 | 0.10 | 0.45 |
| *V*11 | 0.3 | 0.45 | 34.3 | 0.1 | 0.20 | 0.45 |
| *V*12 | 0.3 | 0.45 | 34.3 | 0.1 | 0.30 | 0.45 |
| *V*13 | 0.3 | 0.45 | 34.3 | 0.1 | 0.40 | 0.45 |
| *V*14 | 0.3 | 0.45 | 34.3 | 0.1 | 0.60 | 0.45 |
| *V*15 | 0.5 | 0.35 | 55.3 | 0.1 | 0.10 | 0.35 |
| *V*16 | 0.5 | 0.35 | 55.3 | 0.1 | 0.50 | 0.35 |
| *V*17 | 0.6 | 0.30 | 67.1 | 0.1 | 0.60 | 0.30 |

1280 particles for model M4.

The simulation method of Alder *et al.*[45] is applied. It is an event-driven molecular dynamics procedure for piecewise-continuous potentials of single particles[46,47] and molecules.[43,44] Given the positions, velocities and interaction potentials, this procedure is based on the calculation of collision times for every pair of particles. Between collisions, all the particles move with constant velocity. The pair with the minimum collision time is selected: these particles collide and exchange energy and linear momentum in accordance with their conservation laws. Collision times are updated for the two particles that just collided and the process starts again selecting the new minimum collision time. Time saving schemes such as the Verlet list or the nearest cell[48,49] are applied. The temperature is kept constant with a velocity scaling scheme applied every 100 collisions.

The simulation box is elongated ($L^*_x = 2L^*_y$), where $L^*_y$ is between 13.9 and 27.7 for model M2, and in the range from 14.6 to 25.3 for model M4. This geometry is used in order to try to pinpoint the coexistence of the kagome lattice with fluid phases, applying the spinodal decomposition procedure first used by Chapela *et al.*[50] for a liquid-vapor orthobaric curve of a SW in 3D, and recently applied to crystal phases of a SW in 2D.[51] This procedure consists in simulating isochores at different temperatures to obtain the density profiles of the two phases in equilibrium. When dealing with a liquid-vapor orthobaric curve, it is advisable to use a density close to the critical one. For the solid-fluid orthobaric, several isochors are used to obtain the whole span of the orthobaric curve. The selected number of isochors and temperatures of each density depends on the degree of accuracy desired. It is found that three isochores are sufficient to obtain an acceptable span of the orthobaric curve. When two phases are in equilibrium in the simulation cell, the densities of the two phases are obtained from the corresponding density profiles and plotted in a phase diagram. Other points are obtained as the frontier of the region where the simulation box contains only one phase, indicating that at those conditions the system is outside (above) the orthobaric curve.

Isochores $\rho^* = 0.2$, 0.4 and 0.6 are simulated. The temperature is changed, in increments of 0.05, from $T^* = 0.05$ up to 0.4 for the two smaller densities, and up to 0.5 for the larger one. For both models, blocks of 25 million collisions each are performed. For model M2, 34 to 50 blocks are done; for M4, 62 to 75 blocks are accumulated. Simulations with a larger box and larger number of molecules (1024 molecules with 5120 particles for model M4) are performed to test that the properties calculated in this work, such as orthobaric densities and structural quantities like the radial distribution functions, are not sensitive to the finite size of the system. A further refinement of the temperatures was carried out, at intervals of 0.015, for $0.100 < T^* < 0.205$ at the first two densities, and for $0.150 < T^* < 0.255$ at $\rho^* = 0.6$. The results after 100 blocks of 25 million collisions are not sensitive to this increase in size, as expected. Still, a full finite-size scaling analysis is not attempted at this stage.

## 4 Results

### 4.1 Model M2 without HD sites

No versions of model M2 ever formed a kagome lattice. Versions V6 and V7 with the largest ranges ($\lambda^*_{SW} = 0.7$ and 0.8) formed very interesting linear angled structures for a wide range of density and temperature, where the patchy molecules integrate themselves into long linear polymers which suddenly form angles. An example of these formations is depicted in Fig. 2. For V6 and V7, the angles spanned by the attractive potential are above 65 degrees, which is beyond the maximum limit required for the formation of triangles[3]. The vibrational nature of the attractive sites allow them to move to one side of the molecule, in a polarized-like configuration that permits multiple bonding, favoring the formation of linear structures over the kagome lattice. Once the linear aggregates are formed, the attractive sites are no longer available for further association; therefore, the assemblies behave as double-HD chains. As mentioned earlier, Preisler *et al.*[32] found, using a cluster-size distribution analysis, that linear aggregates of one-patch molecules in 3D are metastable with respect to lamellar structures; it would be useful to investigate the stability of the 2D aggregates using a similar method. A thorough study of such assemblies of flexible molecules is being prepared for future publication.

To further test the stability or instability of kagome lattices for model M2, version V1 is simulated starting from a per-

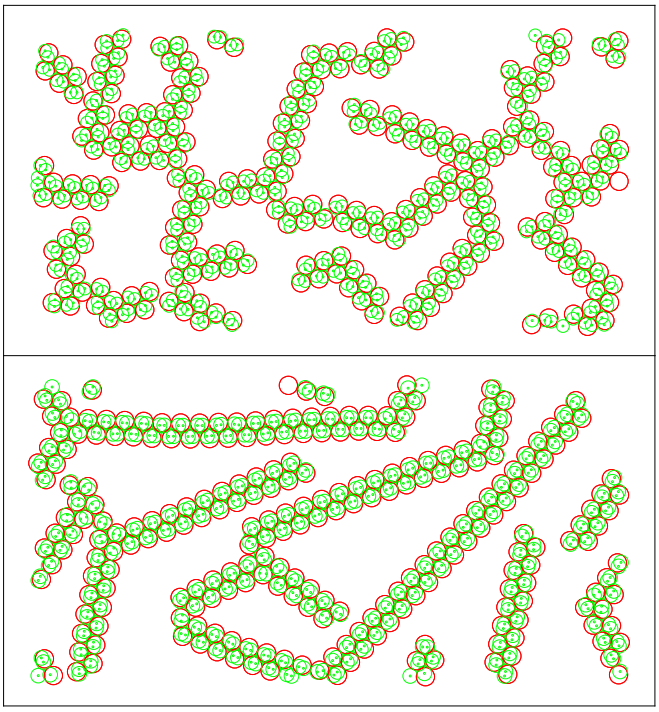

**Fig. 2** Linear structures formed by model M2 with attractive SW sites only (versions V6 and V7, given in Table 1). The density for both states is $\rho^* = 0.5$, the temperatures are $T^* = 0.3$ for V6 at the top panel and $T^* = 0.16$ for V7 at the bottom.

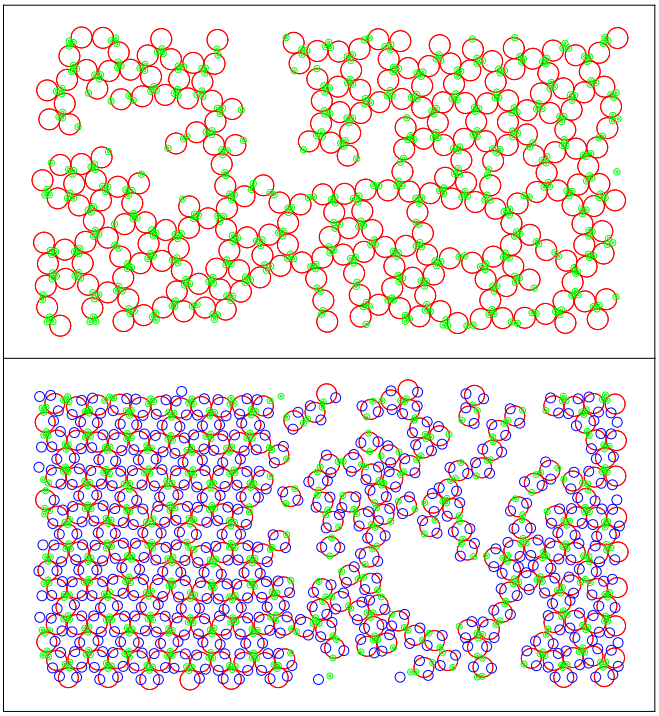

**Fig. 3** Comparison of the disordered fluid obtained with model M2 (top, version V1 in Table 1) and the kagome-fluid coexistence obtained for model M4 with hard-disk sites (bottom, version V8 in Table 2). For the figure on top, $\rho^* = 0.67$ and $T^* = 0.15$; for the figure below, $\rho^* = 0.6$ and $T^* = 0.2$.

fect kagome-lattice configuration. This time, the isochore $\rho^* = 0.6$ is followed, with temperatures ranging from $T^* = 0.05$ to 0.4, at intervals of 0.05. At higher temperatures, $T^* > 0.1$, the kagome lattice is destroyed; only for the two lowest temperatures (0.05 and 0.10) a disordered lattice prevailed with very distorted hexagonal motifs. Therefore, it is inferred that a perfect kagome lattice is not just difficult to obtain kinetically, but is probably unstable at the conditions described above.

### 4.2 Model M4 with HD sites

Since model M2 did not lead to spontaneous formation of kagome lattices, the second model M4 is tried. For simplicity, unless other versions are explicitly stated, M4 refers to its basic form, named version V8, and M2 refers to version V1. The effect of the additional vibrating HD sites, which renders the excluded volume anisotropic, is striking: model M4 was found to produce kagome lattices over wide ranges of temperature and density. Fig. 3 shows the contrast between two configurations obtained at similar state points of density $\rho^*$ and temperature $T^*$ with the two types of models, $(\rho^*, T^*) = (0.67, 0.15)$ for M2 and (0.60, 0.20) for M4. Only the latter system forms a kagome lattice, while just a few deformed hexagonal pores are noticeable in the former.

The percentage of molecules in triangular and hexagonal clusters are used to quantify the difference between these two configurations: while the triangular cluster percentage is about the same in the two cases (87% for M2 and 83% for M4), the percentage of hexagons is clearly smaller for M2 (31%) than for M4 (63%). For an ideal kagome lattice these percentages should be 100%; the reason why the configuration for M4 does not reach these values is not the presence of defects, rather it is due to an equilibrium between the kagome structure and a fluid composed of linear arrays of patchy molecules. In the bottom panel of Fig 3 one can see that the elongated simulation box allowed the formation of an interface between these two phases, so the phase diagram is explored, as it is next described.

### 4.3 Phase diagram for model M4

The phase diagram of model M4 is shown in Fig. 4, indicating the coexistence densities of a fluid and a denser kagome lattice. The three isochores $\rho^* = 0.2$, 0.4 and 0.6 were followed as the temperature changed from $T^* = 0.05$ to 0.25, with in-

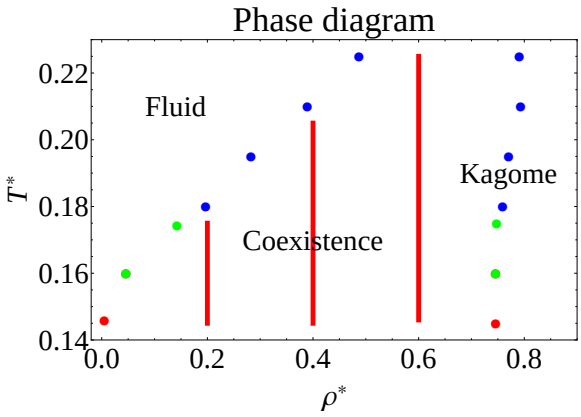


**Fig. 4** Phase diagram $T^*$ *vs.* $\rho^*$ for model M4. Dots are kagome-fluid phase equilibrium points. The vertical bars indicate the regions of the starting isochores $\rho^* = 0.2, 0.4$, and 0.6 where a kagome lattice was found in equilibrium with a fluid.

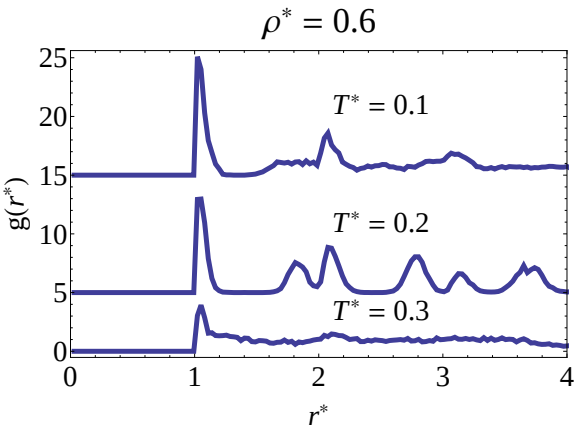


**Fig. 6** Radial distribution functions for model M4 at $\rho^* = 0.6$. At $T^* = 0.3$, the structure is consistent with a fluid phase. For $T^* = 0.2$, sharp peaks corresponding to a kagome lattice are observed. At $T^* = 0.1$, the system fails to form an ordered network.

crements of 0.05. The vertical bars in Fig. 4 indicate the region of these isochores where the kagome lattice was found in equilibrium with a fluid. To facilitate the reading of Fig. 4, a series of typical configurations corresponding to these equilibrium conditions are shown in Fig. 5.

At the highest temperature shown in Fig. 5, $T^* = 0.25$, the system remains in a single phase: a vapor composed mostly of single molecules for $\rho^* = 0.2$, a denser fluid formed by long chains of molecules for $\rho^* \geq 0.4$. As the temperature goes down, a coexistence arises between a fluid phase and a kagome lattice: for instance, at $T^* = 0.2$ and the highest density $\rho^* = 0.6$, the system shows a beautiful kagome lattice coexisting with a fluid formed by long chains of molecules (see the extreme right of the second row from the top in Fig. 5).

The density of the coexisting fluid decreases with decreasing temperature, while that of the kagome lattice remains largely unaffected. Thus, the overall shape of the orthobaric is very similar to the envelopes presented by Romano *et al.*[33] for kagome lattices formed by triblock Janus particles. No fluid-fluid coexistences nor critical point were found. The exploration of the higher density region ($\rho^* > 0.8$) did not find any closed-packed crystal, since the vibrating HD sites prevent the formation of such a closed-packed array.

In contrast with the phase diagram of Romano *et al.*,[33] the region with kagome lattice formation does not extend to low temperatures. At $T^* = 0.10$ (second row from the bottom in Fig. 5), the kagome lattice is not well formed. Under these conditions, the characteristic hexagonal motifs of the kagome lattice coexist with many other closed structures in a disordered way. At $T^* = 0.05$ and the lowest density $\rho^* = 0.2$, a set of fibers are formed with a small number of closed loops. Increasing the density at the same temperature yields the same long fibers, but with an increased amount of loops. Once more, it is possible that these structures are metastable with respect to other morphologies: besides studying their relative free energy, further simulation work may be helpful to characterize the kinetics of formation of the kagome lattice and the linear fibers.

### 4.4 Structure and kinetics of lattice formation

The radial distribution function of the system gives further evidence of the formation of the kagome lattice. In Fig. 6, three radial distribution functions are given for the isochore $\rho^* = 0.6$ at $T^* = 0.1$, 0.2 and 0.3. For the highest temperature, the radial distribution function, with no sharp peaks beyond first neighbors, corresponds to a fluid-like structure. At the middle temperature, $T^* = 0.2$, the full kagome network has developed: the second and third peaks, corresponding to the existence of an hexagonal lattice, are appreciable and resolved fully as distinct peaks. The structure for the lowest temperature, $T^* = 0.1$, corresponds to a configuration where some cycles have begun to develop, but they fail to form an ordered network and may not be at equilibrium. (This configuration is shown at the far right of the second row from the bottom in Fig. 5).

As the simulation uses a Molecular Dynamics method, the time evolution of the system can be followed directly. The time evolution of the amount of single molecules and the formation of pairs, triangles and hexagons is calculated. Fig. 7 is a plot of the percentage of each of these structures against the logarithm of $t^*$, the reduced time since initialization, for the state with $\rho^* = 0.6$ and $T^* = 0.18$. In the initial stages of the simulation there are many isolated molecules and very few of the other structures. Next, pair formation takes off, reaching a maximum about 65%, while the number of isolated molecules

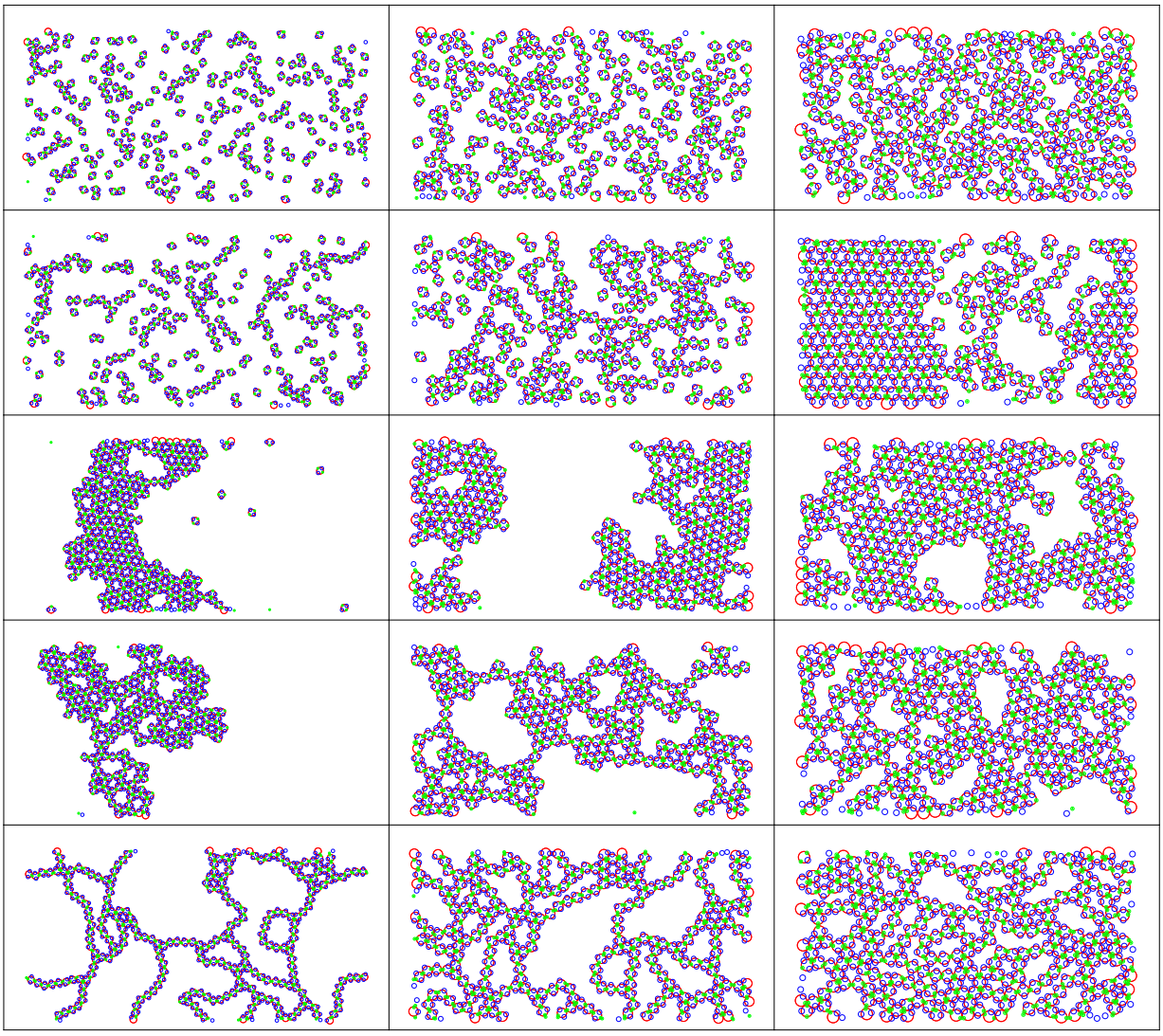

**Fig. 5** Configurations for model M4 at the three isochores $\rho^* = 0.2$, 0.4 and 0.6, for each column from left to right, respectively. Temperatures are $T^* = 0.05$ to 0.25, with increments of 0.05 for each row from bottom to top. At the highest temperatures, only one fluid phase is present. At intermediate temperatures, coexistence between a kagome lattice and a fluid was observed. At the lowest temperatures, no kagome lattice was found; instead disordered linear structures with abundant loops are obtained.

decreases very rapidly. Then the formation of triangles starts to increase rapidly while the amount of pairs decreases until the end of the run. In the last stage, the formation of hexagons starts to increase until the lattice is complete. The time evolution shown in figure Fig. 7 is very similar to that published for isolated, chain- and triangular-bonded particles by the experimental group of Chen *et al.*[3], the configuration-space Monte Carlo results by Romano *et al.*.[33] and the Dissipative Particle Dynamics (DPD) findings of Arai *et al.*[9] The dynamics of hexagonal motifs, however, was not presented in those studies. It will be shown in the next section that the formation of hexagons can be low even if the formation of triangular motifs is high; therefore, it is important to monitor the slow formation of hexagonal motifs during the growth of the kagome lattice.

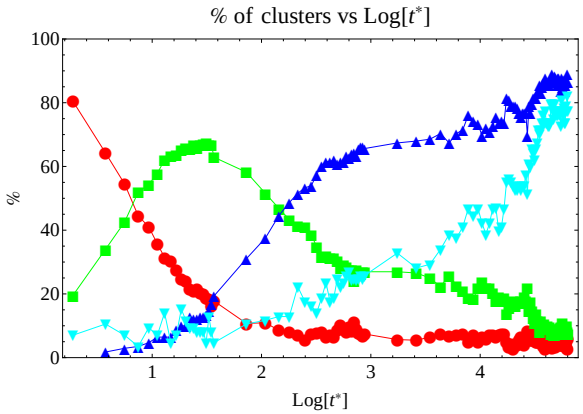


**Fig. 7** Dynamical evolution of a kagome lattice for M4, expressed as percent of patchy molecules forming clusters of 1, 2, 3 or 6 elements as a function of the logarithm of reduced time, $t^*$: red circles represent the percentage of isolated molecules; green squares, pairs of patchy molecules; blue triangles, ternary arrays; and cyan inverted triangles, hexagonal motifs.

### 4.5 Effects of HD size and SW attractive range

The difference between models M4 and M2 is the presence of vibrating HD sites with a diameter $\sigma^*_{HD} = 0.5$. To test how important for the formation of kagome lattices is the size of these HD sites, simulations for versions V9 to V14 of model M4 are performed, which differ from V8 only by the value of their HD-site diameter: $\sigma^*_{HD} = 0.01, 0.1, 0.2, 0.3, 0.4, 0.5$, and 0.6.

Fig. 8 shows the effect of varying the HD-site diameter on the percentage of triangles and hexagons formed by the end of the simulation. For the majority of intermediate diameters, percentages are quite similar to the values obtained for the original version V8: between 87% and 89% for triangles and between 75% and 82% for hexagons. For version V14 with the largest diameter, $\sigma^*_{HD} = 0.6$, a dramatic fall in the percentage

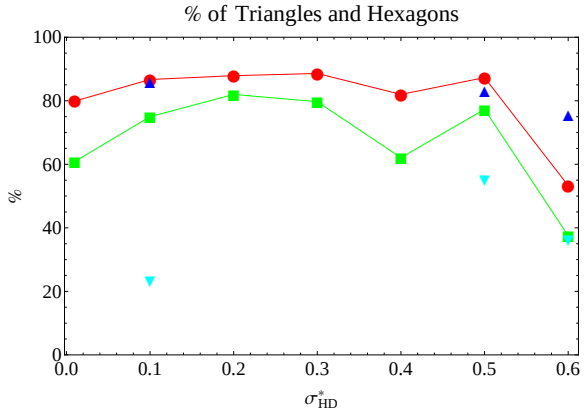


**Fig. 8** Percentage of patchy molecules forming clusters of three and six elements for different versions of M4 with varying HD-site diameter, $\sigma^*_{HD} = 0.01$, 0.1, 0.2, 0.3, 0.4, 0.5 and 0.6. For versions V8 to V14: red circles represent clusters of three molecules; green squares, hexagonal motifs. For versions V15 to V17: blue triangles represent triangular clusters, while cyan inverted triangles correspond to clusters of six molecules. Systems with low formation of hexagonal motifs do not form kagome lattices readily.

of both triangles and hexagons is observed due to the fact that for this diameter the HD sites strongly prevent the formation of hexagonal motifs and the kagome structure. Version V9, with the very small diameter $\sigma^*_{HD} = 0.01$, is puzzling because its percentages of triangles and hexagons are rather high (80% and 61%, respectively). Even though both values are lower than those for $\sigma^*_{HD} = 0.4$, they are not as low as for $\sigma^*_{HD} = 0.6$ (53% for triangles and 37% for hexagons), which are way down the values for the other, kagome-forming systems.

Since $\sigma^*_{HD} = 0.1$ is already a small diameter, the question whether the effect of the vibrating HD sites is due to excluded volume or vibration has to be addressed. To do this, a simulation was performed for version V15, which has the vibrating repulsive sites completely hidden inside the central HD ($\sigma^*_{HD} = 0.10$ and $L^*_{HD} = 0.35$), but still with the opening angle $\theta_{SW}$ below the 65 degree limit. The resulting percentages of triangles and hexagons were 86% and 23%, respectively. Even though the triangle formation is right, the hexagons formation is severely depressed with respect to that seen for version V9 at the same HD-site diameter (see Fig. 8): this shows that vibration alone does not account for the stabilization of the hexagonal motifs in our vibrating patchy-molecule model, so this might be possibly due to an excluded-volume effect.

The vibrating patchy molecules are flexible, therefore, there is room for compressing the HD sites against the central core when model M4 forms assemblies. To check for this, for each system with increasing diameter $\sigma^*_{HD} = 0.01, 0.1, \ldots, 0.6$, the instantaneous protrusion of the vibrating HD sites is averaged and obtained the values $\langle \delta^*_{HD} \rangle = 0.003$, 0.02, 0.04, 0.09, 0.14,

0.19, and 0.24, respectively. In addition, the percentage of configurations with positive HD protrusion was 4% and 36% for the systems with $\sigma^*_{HD}$ = 0.01 and 0.1 and 100% for all other systems. These results indicate that the HD sites are only slightly compressed for the systems with HD diameter above 0.1 but they are actually "expanded" for the two smaller-diameter cases.

Finally, two last versions of model M4 (V16 and V17) are simulated to show the effect of the attractive SW range. The results are shown in Fig. 8 at $\sigma^*_{HD}$ = 0.5 and 0.6, respectively. Just like for version V15, it is clear that neither of these models form a kagome lattice because, while triangle formation is high (83% for V16 and 76% for V17), hexagons are rarely formed (55% for V16 and 36% for V17). Taken together, these tests indicate that formation of hexagonal motifs for model M4 with $\lambda^*_{SW} = 0.3$ is robust to changes of the HD-site diameter, but sensitive to changes of the attractive SW range. Thus, model M4 seems close to an optimal model for kagome-lattice formation with vibrating patchy molecules in two dimensions.

## 5 Conclusions

A simple two-dimensional model, formed by a central hard core decorated by vibrating interaction sites is presented. It provides a useful addition to the understanding of thermodynamic conditions and time evolution of the self-assembly process of kagome lattices and linear structures.

The versions with two attractive SW sites only (model M2) did not lead to formation of kagome lattices. Instead, the attractive sites were displaced away from their center of vibration, into a polarized-like configuration. Thus, the flexibility introduced in the model resulted in the formation of triangular motifs with the attractive sites hidden into the central cores, which allow multiple bonding between patches. Since multiple bonding is energetically favorable, the molecules of model M2 combined into linear arrays, preventing the formation of a closed-pack or a kagome lattice. Further analysis is needed to determine whether these linear structures are stable or metastable only.

Many versions with two attractive and two repulsive sites (model M4) did form kagome lattices. The simulations show the coexistence of the kagome lattice and a fluid over wide ranges of temperature and density, but they did not show any fluid-fluid coexistence nor formation of a closed-pack crystal. The latter solid was prevented because the extra repulsive sites exclude closed-pack configurations specifically. At the lowest simulated temperatures and intermediate densities, instead of fluid-solid coexistence, the formation of disordered networks of looping structures is observed, which may be metastable too. The abundance of loops in these networks increased with density at constant temperature.

It is found that there is a large range of repulsive-site diameters that result in model M4 forming a large amount of the hexagonal motifs required to assemble a kagome lattice, but increasing the range of the attractive SW rapidly inhibits the formation of that open lattice. Formation of the hexagonal motifs was also inhibited when the repulsive sites only had a vibrational role (hidden inside the central core), so it may be concluded that the main effect arises from steric hindrance. A small diameter, such as $\sigma^*_{HD} = 0.01$, is sufficient to promote the formation of the hexagonal motifs; even so, the HD sites deviate only slightly from their center of vibration in the kagome lattices. This prompts us to ask, especially for the design of molecular-sized systems able to form open lattices, whether one could ignore the role of solvent structure near particle surfaces: the density profile would have strong oscillations leading to effective attraction or repulsion for distances on the order of a few molecule diameters. Comparing simulations that deal explicitly and effectively with these interactions would clarify the matter.

Even though model M4 presented in this work and the triblock model studied by Romano *et al.*[33] have similar opening angles ($\theta_{SW}$ = 34.3 for M4 and $\theta_{SW}$ = 32.9), they show some differences in their behavior: they have similar fluid-kagome lattice coexistence envelopes, but model M4 does not form a closed-pack crystal at high densities nor a kagome lattice at low temperatures, where it displays entangled webs of linear structures. These differences represent a good opportunity for testing and developing theories of lattice stability,[23,24] kinetics of formation of stable *vs.* metastable morphologies,[32] as well as mechanical response.[52]

## Acknowledgments

The authors acknowledge the support of the Super Computing Center of UAM Iztapalapa for a generous allotment of computing time. JAM-G is grateful for a posdoctoral scholarship from CONACYT grant 168001 "Efecto de la quiralidad, polaridad y anisotropía en el auto-ensamblaje molecular en dos dimensiones".

## Appendix

The interaction potential between two vibrating patchy molecules $m$ and $n$, each with a number $n_p$ of patches, can be written as

$$U(m,n) = U_{\mathrm{HD}}(\mathbf{r}_{mn}) + \sum_{i=1}^{n_p-1}\sum_{j=i+1}^{n_p} U_{\mathrm{S}}(\mathbf{r}^{ij}_{mn}) + \sum_{k=1}^{n_p-1}\sum_{l=k+1}^{n_p} U_{IN}(\mathbf{r}^{kl}_{mm}). \quad (1)$$

The hard-disk potential $U_{\rm HD}$ depends on $\mathbf{r}_{mn}$, the distance between the centers of the hard-disk cores belonging to molecules $m$ and $n$:

$$U_{\rm HD} = \begin{cases} \infty & \|\mathbf{r}_{mn}\| \leq \sigma, \\ 0 & \|\mathbf{r}_{mn}\| > \sigma. \end{cases} \quad (2)$$

The site potential $U_S$ is a function of $\mathbf{r}^{ij}_{mn}$, the distance between sites $i$ and $j$ of different molecules $m$ and $n$:

$$U_{\rm S} = \begin{cases} -\varepsilon_{SW} & \|\mathbf{r}^{ij}_{mn}\| \leq \lambda_{SW}, \\ 0 & \|\mathbf{r}^{ij}_{mn}\| > \lambda_{SW}. \end{cases} \quad (3)$$

In this work, all attractive SW sites have range $\lambda_{SW}$ and depth $\varepsilon_{SW}$, while all HD sites have zero depth.

Infinite SW potentials are used as intramolecular potentials,[53] where the patches that decorate the central HD are trapped and allowed to vibrate, rattling back and forth between two infinite SW walls. $U_{IN}$ is the intramolecular-trapping potential well that depends on $\mathbf{r}^{kl}_{mm}$, the distance between sites $k$ and $l$ of the same molecule $m$:

$$U_{\rm IN} = \begin{cases} \infty & L - L_{VW}/2 \leq \|\mathbf{r}^{kl}_{mm}\|, \\ 0 & L - L_{VW}/2 \leq \|\mathbf{r}^{kl}_{mm}\| < L + L_{VW}/2, \\ \infty & \|\mathbf{r}^{kl}_{mm}\| > L + L_{VW}/2. \end{cases} \quad (4)$$

$L_{VW}$ sets the maximum amplitude of the intramolecular vibration for the trapping SW centered at $L$.

The bottom part of Fig. 1 shows representations of the trapping potentials used in models M2 and M4. At the left, for model M2, the left-most infinite well (centered at $L_{SW}$) is used to trap each of the two patches to the central HD; the second infinite well traps the SW sites to each other at an average distance of $2L_{SW}$. At the right, for model M4, the first infinite well (again centered at $L_{SW}$) traps the two SW sites to the central HD; the second infinite well traps every SW site to each HD site at an average distance of $\sqrt{(2L^2_{SW})} \approx 0.65$; finally, two other infinite wells trap the SW sites with each other at an average distance of $2L_{SW}$ and the HD sites with each other at an average distance of $2L_{HD}$

## References


1 G. M. Whitesides and B. Grzybowski, *Science*, 2002, **295**, 2418.
2 I. Syosi, *Prog. Theo. Phys.*, 1994, **VI**, 306.
3 Q. Chen, S. C. Bae and S. Granick, *Nature*, 2011, **469**, 381–384.
4 Y. Xia, Y. Yin, Y. Lu and J. McLellan, *Adv. Funct. Mater.*, 2003, **13**, 907.
5 Q. Chen, E. Diesel, J. K. Whitmer, S. C. Bae, E. Luijten and S. Granick, *Journal of the American Chemical Society*, 2011, **133**, 7725–7727.
6 Q. Chen, J. Yan, J. Zhang, S. C. Bae and S. Granick, *Langmuir*, 2012, **28**, 13555–13561.
7 Q. Chen, S. C. Bae and S. Granick, *Journal of the American Chemical Society*, 2012, **134**, 11080–11083.
8 X. Cheng, X. Xu, S. A. Rice, A. R. Dinner and I. Cohen, *Proceedings of the National Academy of Sciences*, 2012, **109**, 63–67.
9 N. Arai, K. Yausoka and X. C. Zeng, *Journal of Chemical Theory and Computation*, 2012, **9**, 179–187.
10 K. Chaudhary, Q. Chen, J. J. Jua rez, S. Granick and J. A. Lewis, *Journal of the American Chemical Society*, 2012, **134**, 12901–12903.
11 Z. He and I. Kretzschmar, *Langmuir*, 2012, **28**, 9915–9919.
12 Z. Zhao, Z. Shi, Y. Yu and G. Zhang, *Langmuir*, 2012, **28**, 2382–2386.
13 D. J. Kraft, R. Ni, F. Smallenburg, M. Hermes, K. Yoon, D. A. Weitz, A. van Blaaderen, J. Groenewold, M. Dijkstra and W. K. Kegel, *Proceedings of the National Academy of Sciences*, 2012, **109**, 10787–10792.
14 M. Motornov, S. Z. Malynych, D. S. Pippalla, B. Zdyrko, H. Royter, Y. Roiter, M. Kahabka, A. Tokarev, I. Tokarev, E. Zhulina *et al.*, *Nano letters*, 2012, **12**, 3814–3820.
15 S. Sacanna, L. Rossi and D. J. Pine, *Journal of the American Chemical Society*, 2012, **134**, 6112–6115.
16 A. Chakrabarty, F. Wang, C.-Z. Fan, K. Sun and Q.-H. Wei, *Langmuir*, 2013, **29**, 14396–14402.
17 W. Gao, A. Pei, X. Feng, C. Hennessy and J. Wang, *Journal of the American Chemical Society*, 2013, **135**, 998–1001.
18 A. A. Shah, B. Schultz, K. L. Kohlstedt, S. C. Glotzer and M. J. Solomon, *Langmuir*, 2013, **29**, 4688–4696.
19 X.-W. Xu, X.-M. Zhang, C. Liu, Y.-L. Yang, J.-W. Liu, H.-P. Cong, C.-H. Dong, X.-F. Ren and S.-H. Yu, *Journal of the American Chemical Society*, 2013, **135**, 12928–12931.
20 Y. Wang, Y. Wang, X. Zheng, G.-R. Yi, S. Sacanna, D. J. Pine and M. Weck, *Journal of the American Chemical Society*, 2014.
21 C. Lu and M. W. Urban, *ACS Macro Letters*, 2014, **3**, 346–352.
22 Q.-N. Zheng, L. Wang, Y.-W. Zhong, X.-H. Liu, T. Chen, H.-J. Yan, D. Wang, J.-N. Yao and L.-J. Wan, *Langmuir*, 2014, **30**, 3034–3040.
23 X. Mao, Q. Chen and S. Granick, *Nature Materials*, 2013, **12**, 217.
24 X. Mao, *Phys. Rev. E*, 2013, **87**, 062319.
25 E. Edlund, *PhD Thesis, Chalmers University of Technology*, 2014.
26 H. Shin and K. S. Schweizer, *Soft matter*, 2014, **10**, 262–274.
27 G. Doppelbauer, E. G. Noya, E. Bianchi and G. Kahl, *Soft Matter*, 2012, **8**, 7768–7772.
28 M. N. van der Linden, J. P. Doye and A. A. Louis, *The Journal of chemical physics*, 2012, **136**, 054904.
29 F. Leoni and G. Franzese, *arXiv preprint arXiv:1406.1996*, 2014.
30 Z.-W. Li, Z.-Y. Lu, Z.-Y. Sun and L.-J. An, *Soft Matter*, 2012, **8**, 6693–6697.
31 Z.-W. Li, Z.-Y. Lu, Y.-L. Zhu, Z.-Y. Sun and L.-J. An, *RSC Advances*, 2013, **3**, 813–822.
32 Z. Preisler, T. Vissers, F. Smallenburg, G. Munao and F. Sciortino, *The Journal of Physical Chemistry B*, 2013, **117**, 9540–9547.
33 F. Romano and F. Sciortino, *Soft Matter*, 2011, **7**, 5799–5804.
34 F. Romano and F. Sciortino, *Nature communications*, 2012, **3**, 975.
35 Y. Li, Y. Zhu, Y. Li, H. Qian and C. Sun, *Molec. Simul.*, 2014, **40**, 449.
36 W. L. Miller and A. Cacciuto, *Soft Matter*, 2011, **7**, 7552.
37 M. Lattuada and T. A. Hatton, *Nano Today*, 2011, **6**, 286–308.
38 A. Nych, U. Ognysta, M. Škarabot, M. Ravnik, S. Žumer and I. Muševič, *Nature communications*, 2013, **4**, 1489.
39 S. Sacanna, M. Korpics, K. Rodriguez, L. Colón-Meléndez, S.-H. Kim, D. J. Pine and G.-R. Yi, *Nature communications*, 2013, **4**, 1688.
40 G.-R. Yi, D. J. Pine and S. Sacanna, *Journal of Physics: Condensed Matter*, 2013, **25**, 193101.
41 E. Edlund, O. Lindgren and M. N. Jacobi, *Phys. Rev. Lett.*, 2011, **107**, 085503.
42 A. Giacometti, F. Lado, J. Largo, Pastore, G. and F. Sciortino, *J. Chem. Phys.*, 2010, **132**, 174110.
43 G. A. Chapela and J. Alejandre, *J. Chem. Phys.*, 2010, **132**, 104704.
44 G. A. Chapela and J. Alejandre, *J. Chem. Phys.*, 2011, **135**, 084126.
45 B. J. Alder and T. E. Wainwright, *J. Chem. Phys.*, 1959, **31**, 459.

46 D. C. Rapaport, *J. Chem. Phys.*, 1979, **71**, 3299.

47 G. A. Chapela, S. E. Martínez-Casas and J. Alejandre, *Molec. Phys.*, 1984, **53**, 139.

48 P. Allen and D. J. Tildesley, *Computer Simulations of Liquids*, Oxford University Press, New York, 1987.

49 D. Frenkel and B. Smith, *Understanding Molecular Simulation from Algorithms to Applications*, Academic Press, San Diego, 2nd edn, 2002.

50 S. M.-C. G. A. Chapela and C. Barea, *J. Chem. Phys.*, 1987, **86**, 5683.

51 G. A. C. E. V. J. C. Armas-Pérez, 1 J. Quintana-H and G. Navascués, *J. Chem. Phys.*, 2014, **140**, 064503.

52 A. Souslov, J. Liu and T. C. Lubensky, *Phys. Rev. Lett.*, 2009, **103**, 205503.

53 J. C. Armas-Pérez, J. Quintana-H and G. A. Chapela, *J. Chem. Phys.*, 2013, **139**, 024505.